Isotope dependence of the vibrational lifetimes of light impurities in Si from first principles

D. West and S. K. Estreicher*
Physics Department, Texas Tech University, Lubbock, Texas 79409-1051, USA
(Received 12 December 2006; revised manuscript received 2 January 2007; published 23 February 2007)

The vibrational lifetimes of a range of H-related defects and interstitial O (O_i) in Si, including isotopic substitutions, are calculated from first principles as a function of temperature. The theoretical approach is explained in detail. The vibrational lifetimes of highest-frequency local vibrational modes of H_{BC}^{+}, D_2^*, HD^*, DH^*, H_{BC}^{+}, D_{BC}^{+}, $HV\cdot VH$, $DV\cdot VH$, $DV\cdot VD$, IH_2, ID_2, and various O and Si isotopic combinations of O_i are predicted and the decay channels analyzed. We show that the complete vibrational spectrum of the defects must be known in order to predict vibrational lifetimes. We also show that the "frequency-gap law" is not always valid for high-frequency local vibrational modes.

DOI: 10.1103/PhysRevB.75.075206 PACS number(s): 63.20.Mt, 61.72.Bb

I. INTRODUCTION

The relaxation dynamics of impurity-related local vibrational modes (LVMs) in crystals are unexpectedly complex. Indeed, the lifetimes of nearly identical high-frequency modes have been observed to differ by up to 2 orders of magnitude.[1] The great disparity in the observed lifetimes suggests that some LVMs couple to the phonon bath much more efficiently than others, despite their frequencies being nearly identical.

The importance of these issues is illustrated by the passivation by H or D of Si dangling bonds at the Si/SiO_x interface (P_b center).[2,3] The devices treated with D have transconductance lifetimes 10–50 times longer than those treated with H.[4] It is believed that inelastic scattering of hot electrons with the passivated P_b center excites the LVMs of the Si–H or Si–D bonds. If the vibrational lifetime is shorter than the average time between scattering events, the bond remains stable. In the opposite case, the bond is still excited when the next scattering event occurs, and the vibrational energy increases until dissociation occurs. Thus, the dissociation rate depends critically on the vibrational lifetimes.[5]

The lifetimes of H-related stretch LVMs in Si have been measured by transient bleaching spectroscopy.[6,7] At low temperatures, the lifetimes of the 2062 cm^{-1} stretch mode of the H_2^*=Si–$H_{BC}\cdots$Si–H_{AB} pair[1] (the subscripts BC and AB stand for bond centered and antibonding, respectively), the 1998 cm^{-1} asymmetric stretch of H_{BC}^{+},[6,8] and the 2072 cm^{-1} stretch mode of the divacancy-dihydrogen complex[1,9] $HV\cdot VH$ have been measured to be 4, 8, and 295 ps, respectively. Since the optical phonon[10] of Si is around 530 cm^{-1}, it was assumed that these decays should involve at least four phonons, suggesting that all these modes should have long and comparable lifetimes.

Vibrational lifetimes rapidly fall off at high temperatures.[6,7] A general expression[11,12] for the temperature dependence of lifetimes has been used to fit[1,6] the experimental data to the sets of accepting modes. For example, in the case of H_{BC}^{+} the fit yields a six phonon process: three acoustic ($\sim$150 cm^{-1}) and three optic ($\sim$520 cm^{-1}) phonons. A fit using just four accepting modes at 500 cm^{-1} fails to reproduce the data. A good fit is also obtained for the temperature dependence of the lifetime of the $HV\cdot VH$ stretch mode using three acoustic ($\sim$343 cm^{-1}) and two optic ($\sim$520 cm^{-1}) phonons. While good fits can be obtained, they are not unique and the theoretical model fails to explain why an 8 ps lifetime involves six phonons while a 295 ps decay only five.

On the other hand, the measurements of the lifetimes of H-related wag modes[13] yield a more straightforward explanation. The farther away an LVM is from the optical and acoustic phonon bands, the longer the lifetime as the decay involves an increasing number of phonons. The lifetimes increase exponentially with the decay order ("frequency-gap law").

In addition to transient bleaching spectroscopy, lifetimes have been estimated on the basis of linewidth measurements.[6,7,9] The vibrational lifetime is related to the homogenous linewidth[7] $T_1=1/(2\pi c\Gamma_0)$, where Γ_0 is the full width at half maximum at low temperatures and in the low defect concentration limit. Such measurements need to be corrected for both instrumental and inhomogeneous line broadenings.

Previous calculations of vibrational lifetimes in amorphous Si have been done perturbatively[14,15] and by semiempirical molecular-dynamics (MD) simulations.[15] These were performed with a Stillinger-Weber potential[16] at low T and in the limit of small excitations. MD simulations have also been used[17] to calculate the lifetime of Si-H modes on a Si(111) surface, but this was not extended to finite temperatures nor was the initial excitation discussed. A comprehensive review of the approximations involved in earlier calculations of vibrational dynamics is included in Ref. 7.

We have proposed[18] a scheme to calculate vibrational lifetimes at finite temperature from first principles. The initial conditions of the simulation are chosen such that the background temperature of the supercell and the excitation energy of the LVM closely mimic the experimental situation. This scheme was applied to the high-frequency stretch modes of H_2^*, H_{BC}^{+}, and $HV\cdot VH$. It was shown that quantitatively accurate lifetimes for temperatures above $\sim$75 K can be predicted. We have also discussed the isotope dependence of the lifetime of the asymmetric stretch of interstitial O (O_i) in Si.[19] In the present work, we discuss the details of these calculations and present results for more defects and various isotopic substitutions. The role of the complete vibrational

spectra of the defect on the decay mechanisms is discussed.

Section II contains the details of the methodology used to perform the lifetime calculations. Section III describes the calculated lifetimes and, when possible, the decay channels for the highest-frequency LVM of H_{BC}^{+}, D_2^{*}, HD^{*}, DH^{*}, H_{BC}^{+}, D_{BC}^{+}, $HV\cdot VH$, $DV\cdot VH$, $DV\cdot VD$, IH_2, ID_2, and various O and Si isotopic combinations of O_i. Section IV includes a brief summary and a discussion of the main factor governing the lifetime of high- and low-frequency LVMs. In particular, it is shown that *all* the modes localized on the defects can play a key role in the determining vibrational lifetimes, that the frequency-gap law is not always valid as LVMs couple much more strongly to localized than to bulk modes, and that the classical description of the coupled oscillators works remarkably well down to 75 K or so, below which the zero-point motion effects determine the lifetimes.

II. THEORETICAL APPROACH

Our results are based on the SIESTA (Refs. 20 and 21) implementation of MD simulations in 64 host-atom periodic supercells. Norm-conserving pseudopotentials in the Kleinman-Bylander form[22] are used to remove the core regions from the calculations. The valence regions are treated self-consistently within local density-functional theory with the exchange-correlation potential of Ceperley-Alder[23] as parametrized by Perdew-Zunger.[24] The basis sets for the valence states (double zeta in the present work) are linear combinations of numerical atomic orbitals of the Sankey type.[25] The charge density is projected on a real-space grid with equivalent cutoffs of 80 Ry to calculate the exchange-correlation and Hartree potentials. The dynamical matrices are calculated using linear-response theory.[26–28]

The eigenvalues of the dynamical matrix are the normal-mode frequencies ω_s. The corresponding orthonormal eigenvectors $e_{\alpha i}^{s}$ (where $i=x,y,z$) give the relative displacements of the nucleus α for each mode s.

A quantitative measure of how localized a given mode is on an atom or group of atoms is provided by a plot of $L_{\{\alpha\}}^{2}=(e_{\alpha x}^{s})^2+(e_{\alpha y}^{s})^2+(e_{\alpha z}^{s})^2$ vs s or ω_s. $\{\alpha\}$ may be a single atom (e.g., H) or a sum over a group of atoms [e.g., the Si nearest neighbors (NNs) to H]. Such a "localization plot" allows the identification of all the local, pseudolocal (see below), and resonant modes associated with a specific defect.

The eigenvectors $e_{\alpha i}^{s}$ are also needed to transform the (harmonic) normal mode coordinates $q_s=A_s(T)\cos(\omega_s t+\varphi_s)$ into Cartesian nuclear displacements,

$$u_{\alpha i}=\frac{1}{\sqrt{m_\alpha}}\sum_s q_s e_{\alpha i}^{s}.$$

In thermal equilibrium, the *average* kinetic energy of each mode is $k_BT/2$, that is,

$$\left\langle \frac{1}{2}\dot{q}_s^2 \right\rangle = \left\langle \frac{1}{2}\omega_s^2 A_s^2 \sin^2(\omega_s t+\varphi_s)! \right\rangle = \frac{1}{4}\omega_s^2 A_s^2 = \frac{1}{2}k_B T.$$

Thus, the average mode amplitude is given by $\langle A_s\rangle=\sqrt{2k_BT}/\omega_s$. Assigning $A_s=\langle A_s\rangle$ for all s implies that each mode has exactly the energy k_BT. Instead, we use a random distribution,

$$\zeta_s=\int_0^{E_s}\frac{1}{k_BT}e^{-E/k_BT}dE,$$

with $0<\zeta_s<1$ and $A_s=\sqrt{-2k_BT\ln(1-\zeta_s)}/\omega_s$. This results in a random distribution of normal-mode energies, which averages out to k_BT.

Thus, the (harmonic) Cartesian positions and velocities in equilibrium at the temperature T are

$$u_{\alpha i}=\sqrt{\frac{2k_BT}{m_\alpha}}\sum_s\frac{1}{\omega_s}\sqrt{-\ln(1-\zeta_s)}\cos(\omega_s t+\varphi_s)e_{\alpha i}^{s},$$

$$\dot{u}_{\alpha i}=-\sqrt{\frac{2k_BT}{m_\alpha}}\sum_s\sqrt{-\ln(1-\zeta_s)}\sin(\omega_s t+\varphi_s)e_{\alpha i}^{s}.$$

We use these initial ($t=0$) positions and velocities to prepare the supercell in thermal equilibrium at the temperature T. The phases $0\leqslant\varphi_s<2\pi$ are uniformly random: each mode has a random amount of kinetic and potential energies at $t=0$. The LVM under study is assigned the kinetic energy $3\hbar\omega/2$ (zero-point energy plus one phonon). This excitation is achieved using the appropriate eigenvector of the dynamical matrix.

Figure 1 shows test MD runs conducted with a defect-free Si_{64} supercell at 50, 200, and 500 K. The black curves are the temperature of the cell throughout a 10 ps simulation with the initial conditions outlined above, without thermostat. The green (gray) curves show the temperature fluctuations using the conventional method of assigning kinetic energies to each atom from a Maxwell-Boltzmann distribution and with a Nose-Hoover thermostat.[29,30] Note that the larger oscillations in 500 K run suggest that the harmonic approximation assumed here is no longer appropriate.

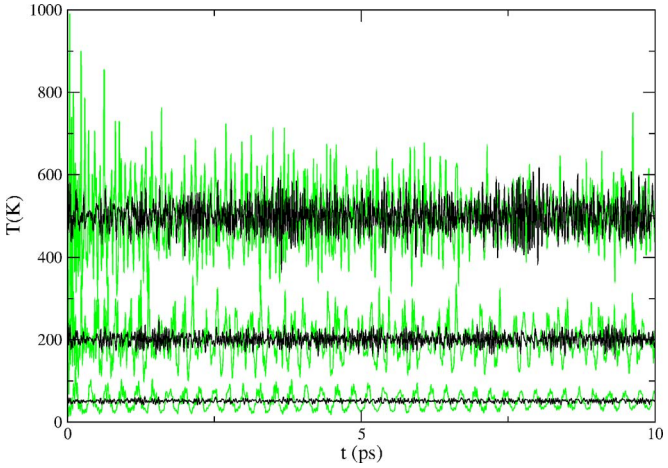

FIG. 1. (Color online) Ten picosecond MD simulation of the defect-free Si_{64} supercell at $T=50$, 200, and 500 K, respectively, with an initial Maxwell-Boltzmann velocity distribution and a Nose-Hoover thermostat (gray or green) vs the initial conditions outlined in this section and no thermostat (black).

Thus, we start a constant-energy MD simulation with the supercell in thermal equilibrium at the temperature T except for the LVM under study, which has $3\hbar\omega/2$ kinetic energy at $t=0$. This excitation redistributes over all the modes of the system as the supercell reaches equilibrium. No thermostat is used since the decay of the LVM would be controlled in part by the thermostat rather than the anharmonic couplings.

Note that there is some ambiguity in what we call the temperature. Indeed, when thermal equilibrium is reached, the temperature of the supercell has increased from T to $T+\Delta T$. In the Si_{64} supercell, ΔT is of the order of 25 K for a mode near 2000 cm^{-1}. In this paper, our results list T (not $T+\Delta T$) as *the* temperature.

The MD run is performed with a time step of 0.3 fs in the case of H-related defects and 1.0 fs in the case of O_i. At every time step, we transform the $3N$ Cartesian coordinates of the N nuclei into linear combinations of the $3N$ normal modes. The amplitudes allow us to calculate the energy (within the harmonic approximation) of every normal mode as a function of (real) time at the temperature T.

In the harmonic approximation, the energy of a normal mode is $E_s=\frac{1}{2}\dot{q}_s^2+\frac{1}{2}\omega_s^2 q_s^2$. The energy of each mode is calculated twice per period, when the normal coordinate q_s associated with that mode is zero. This eliminates the theoretical error in ω_s as well as that associated with ignoring in E_s the terms $\propto q_s^3, q_s^4, \ldots$ and $\propto q_s q_i, q_s q_i q_j, \ldots$.

In the case of LVMs with short lifetimes, the details of the decay process are sensitive to the randomly chosen initial conditions. For this reason, multiple MD runs are performed at each temperature. At each time step, the energy of the LVM is the average of the multiple runs. This averaged decay is then fitted to an exponential which gives the calculated lifetime. An example is discussed below. Note that the longer the lifetime, the less sensitive the decay is to the details of the initial conditions.

In the real crystal, the oscillation amplitudes reach the zero-point values commensurate with the quantum-mechanical ground state as $T\rightarrow 0$. Then, the anharmonic couplings and therefore the lifetimes become constant. On the other hand, in classical MD simulations, the amplitudes of all the modes go to zero, and so do the anharmonic couplings. As a result, the classical lifetimes become very long. Classical MD simulations are unable to reproduce the-low temperature plateau observed for $T_1(T\rightarrow 0)$. Our results are obtained for $T>50$ K.

Finally, note that transient bleaching spectroscopy measures the time needed for the oscillator to return to the ground state, while the theory described here predicts the time needed for the oscillator to leave the excited state. There is a subtle difference here as the former can be limited by the lifetimes of the receiving modes.

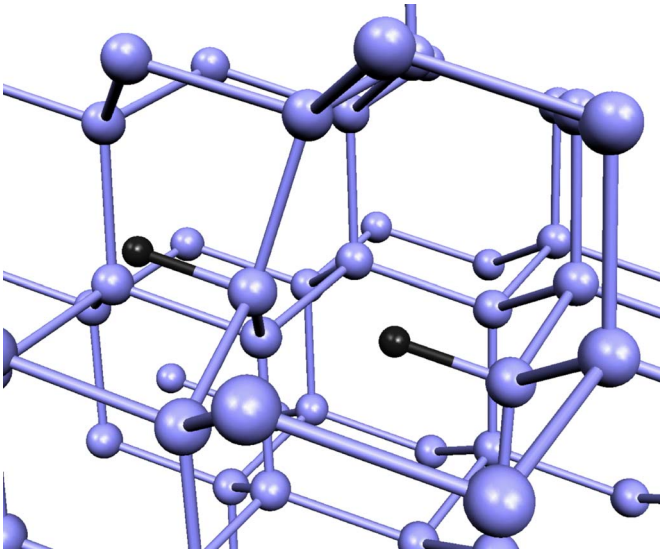

FIG. 2. (Color online) The H_2^* defect consists of H_{BC} and H_{AB} aligned along the same trigonal axis. (Ref. 31).

III. RESULTS

A. Hydrogen-related defects

1. H_2^* and isotope combinations

The H_2^* defect (Fig. 2) consists of H_{BC} and H_{AB} aligned along the same trigonal axis.[31]

The dynamical matrix was calculated for all the isotopic combination: H_2^*, D_2^*, HD^*, and DH^*, where the "*" indicates the BC species. Table I shows the calculated LVMs and their measured values. The calculated frequencies are within a few percent of the experimental ones, which is typical for the relatively small basis set used in the present calculations.

In addition to stretch and wag modes of the impurity atoms, the defect as a whole often introduces pseudolocal modes (pLVMs).[32,33] A pLVM is localized at the defect but has a frequency within the phonon continuum of the crystal. The Si–H_{BC} wag is an example of such a mode.

Figure 3 shows the localization plot $L^2_{\{\alpha\}}(\omega)$ (Sec. II) of H_2^* and its isotope combinations. The solid vertical lines are

TABLE I. Calculated (theor.) and observed (expt. Ref. 31) LVMs for the various isotope combinations of H_2^*.

	BC wag		AB wag		AB stretch		BC stretch	
	Theor.	Expt.	Theor.	Expt.	Theor.	Expt.	Theor.	Expt.
H_2^*	457		853	817	1860	1844	2126	2062
D_2^*	328		611	588	1338	1340	1528	1500
DH^*	457		611		1341		2128	
HD^*	328		856		1519		1879	

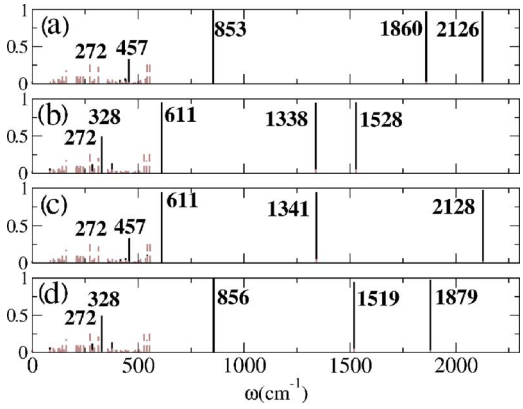

FIG. 3. (Color online) Localization plot $L^2_{\{\alpha\}}(\omega)$ for the different isotopic combinations of H_2^*. $\{\alpha\}$ includes the two H or D (solid lines) or the two NNs Si (dashed lines). (a) is H_2^*, (b) is D_2^*, (c) is DH^*, and (d) is HD^*. The * refers to the BC species.

for α= both H (or D) impurities and the dashed lines are for α=the two Si NNs to H (or D).

The decay of the stretch mode of the BC impurity was calculated at 50, 100, and 150 K for H_2^* as well as 100 and 150 K for D_2^*, HD^*, and DH^*. As explained in Sec. II, multiple MD runs were performed for each isotope combination at each temperature: six for H_2^* (which has the shortest lifetime), three for D_2^*, four for HD^*, and four for DH^*. Figure 4 shows the energy of the Si–H_{BC} stretch mode of H_2^* as a function of time for the six different MD runs performed at 100 K. Although each realization of the decay is far from exponential, the average decay (Fig. 5) nicely fits to an exponential with a time constant of 2.6 ps, in perfect agreement with the measured lifetime at that temperature. In contrast, the decay of the longer-lived DH^* (Fig. 6) reveals very similar decays for all three numerical realizations.

Figure 7 shows that the energy of the Si–H_{BC} LVM at 2062 cm^{-1} decays into the Si–H_{AB} mode (1860 cm^{-1}, solid curve) and a pLVM (271 cm^{-1}, dashed curve). The latter is the symmetric stretch of the two Si NNs of H_2^* (Fig. 3). Thus, the decay of the Si–H_{BC} stretch mode involves two localized

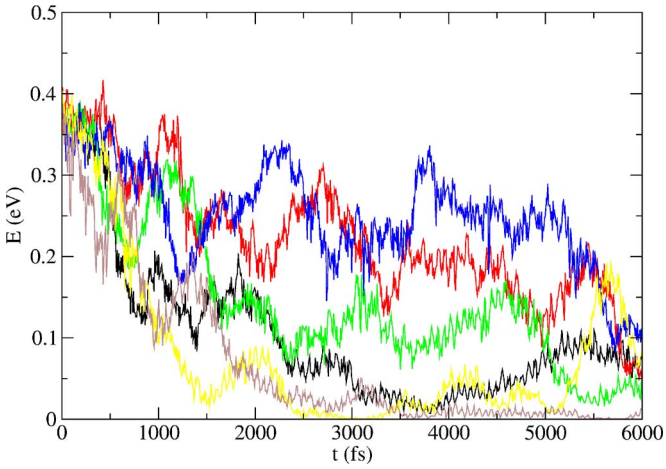

FIG. 4. (Color online) Six different realizations of the decay of the Si–H_{BC} stretch of H_2^* at 100 K (see text).

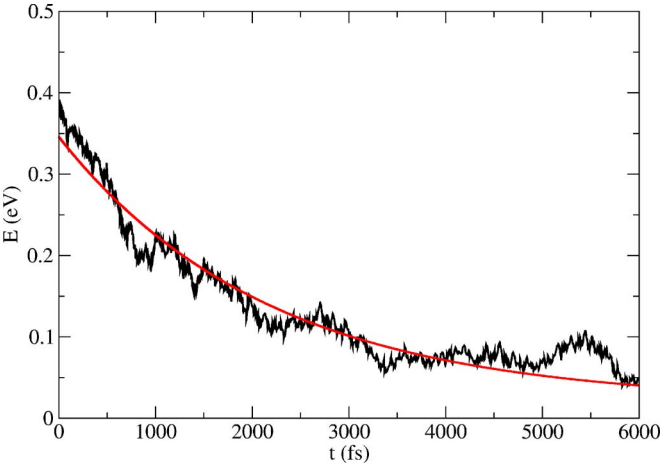

FIG. 5. (Color online) An exponential fit to the step-by-step *average* of the six decays of H_2^* at 100 K (Fig 4) yields a lifetime of 2.6 ps.

modes. It is a two phonon process, not the six phonon process originally suggested.[1]

The calculated lifetimes for the isotope combinations are shown in Table II. For H_2^*, the calculated lifetime of 3.7 ps at 50 K is close to the low-temperature experimental value. The calculated temperature dependence also agrees very well with the measured one. Figure (4) (left) in Ref. 18 compares the calculated lifetimes of 50, 100, and 150 K to the experimental data.[9]

In the case of D_2^*, the calculated lifetime of 18 ps at 100 K is quite a bit larger than the measured low-temperature value of 4.8 ps. The latter was estimated from the linewidth, which tends to underestimate the true value. The discrepancy between theory and experiment may also be due to the finite size of the supercell. Indeed, a two-phonon decay of the 1528 cm^{-1} LVM would require the LVM at 1338 cm^{-1} [see Fig. 3(b)] as well as a bulk phonon near 190 cm^{-1}. The phonon density of states calculated in the Si_{64} has no mode near that value.

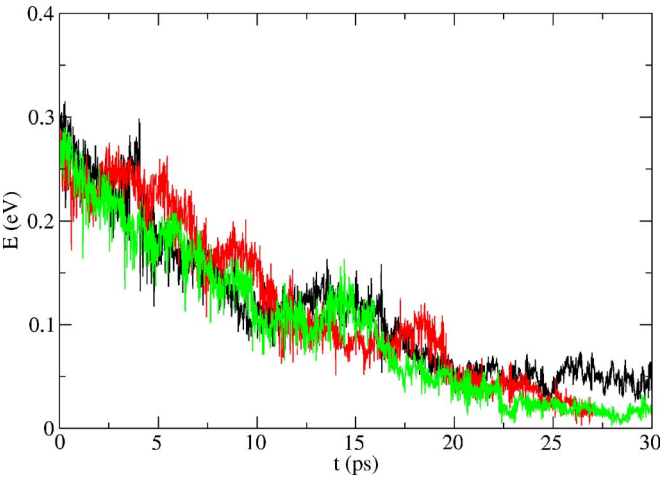

FIG. 6. (Color online) Three realizations of the decay of HD^* at 150 K.

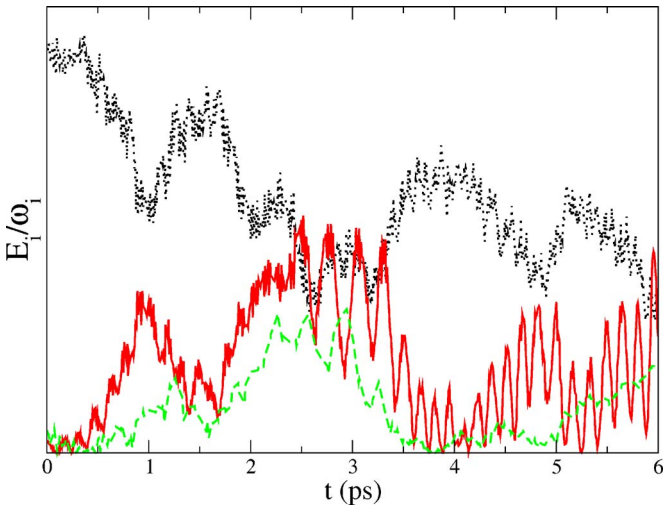

FIG. 7. (Color online) Scaled energies $E(\omega_i)/\omega_i$ of the Si–H_{BC} stretch mode (2062 cm^{-1}, black dotted curve), Si–H_{AB} stretch mode (1860 cm^{-1}, red solid curve), and symmetric stretch of the two Si neighbors in H_2^* (271 cm^{-1}, green dashed curve).

2. H_{BC}^+ and D_{BC}^+

The structure of the H_{BC} is shown in Fig. 8. The calculated frequency of the asymmetric stretch of H_{BC}^+ and D_{BC}^+ are 2014 and 1439 cm^{-1} (measured[34] 1998 and 1449 cm^{-1}), respectively.

The localization plots $L_{\{\alpha\}}^2(\omega)$ of H_{BC}^+ and D_{BC}^+ are shown in Fig. 9. In the case of H_{BC}^+ (top), there are no LVMs other than the asymmetric stretch at 2014 cm^{-1}. Therefore, its decay cannot involve fewer than four phonons and the measured low-temperature lifetime, 7.8 ps, cannot fit on the frequency-gap law. The only localized modes associated with H_{BC}^+ are the asymmetric stretch at 2014 cm^{-1}, the two wag modes (pLVMs) at 261 cm^{-1}, and two NN Si-related pLVMs at 209 and 410 cm^{-1}. The situation is similar for D_{BC}^+ (bottom). The only LVM is the asymmetric stretch of D at 1439 cm^{-1}. The wag modes shift down to 203 cm^{-1} and the Si-related pLVMs at 209 and 409 cm^{-1} remain virtually unchanged relative to H_{BC}^+.

The calculated lifetimes of the asymmetric stretch of H_{BC}^+ are 8.7 ps at 75 K, 5.4 ps at 100 K, and 2.8 ps at 150 K. As shown in Fig. (4) (right) Ref. 18, these lifetimes are close to the measured values.[6] The lifetimes of the same mode of D_{BC}^+ are shorter: 3.9 ps at 100 K and 2.4 ps at 150 K. This is consistent with the fact that the *D*-related LVM is closer to the phonon continuum than the *H*-related one.

TABLE II. Calculated and measured low-temperature lifetimes T_1 (ps) of H_2^* and its isotope substitutions.

Defect	T_1 (50 K)	T_1 (100 K)	T_1 (150 K)	Expt. (<50 K)
H_2^*	3.7	2.6	1.8	4.2[a]
D_2^*		18	14	4.8[b]
DH^*		38	12.8	
HD^*		24	11.6	

[a]Obtained from transient bleaching spectroscopy is (Ref. 1)
[b]Estimated from the linewidth (Ref. 9).

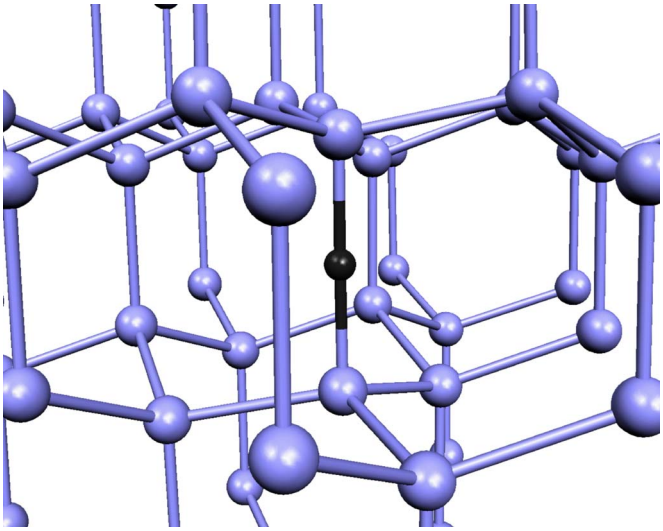

FIG. 8. (Color online) The H_{BC} defect. The H atoms are black and the Si atoms are blue (gray).

Figure (3) Ref. 18 shows the energies of all the normal modes in the supercell vs. time during the decay of the 2014 cm^{-1} mode of H_{BC}^+ at $T=75$ K. The modes whose energies peak sharply and repeatedly throughout the simulation are the 410 cm^{-1} (B) and 261 cm^{-1} (C and D) modes. We performed four MD simulations (each) at $T=50$, 100, and 150 K. The loss of energy in the asymmetric stretch always involves the 410 and 209 cm^{-1} modes, which themselves decay almost immediately into bulk phonon modes. This is apparent in the inset of Fig. (3) in Ref. 18 (12 000 time steps), which shows the inner structure of the B and C peaks.

It appears that the coupling of an LVM to pLVMs is much more efficient than the coupling of an LVM to bulk phonons. This may be due to the fact that pLVMs are strongly localized (Fig. 9) near the defect and therefore involve the motion of very few atoms. This situation is a breakdown of the frequency-gap law.

3. H*V*·*V*H, D*V*·*V*H, and D*V*·*V*D

The lowest-energy structure of the divacancy-dihydrogen H*V*·*V*H defect is shown in Fig. 10. It has C_{2v} symmetry.

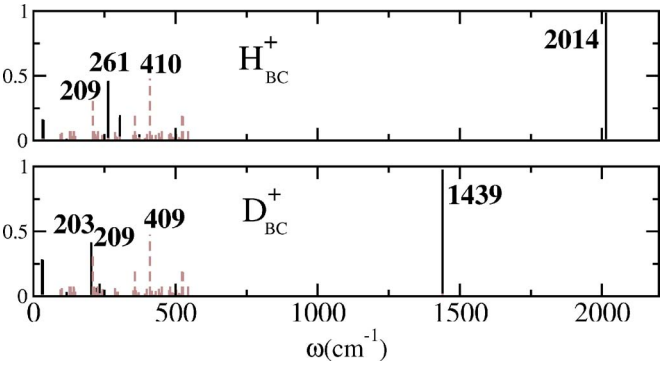

FIG. 9. (Color online) Localization plots $L_{\{\alpha\}}^2(\omega)$ for H_{BC}^+ (top) and D_{BC}^+ (bottom). The solid lines are H (or D)-related modes, and the dashed lines refer to the two Si NNs.

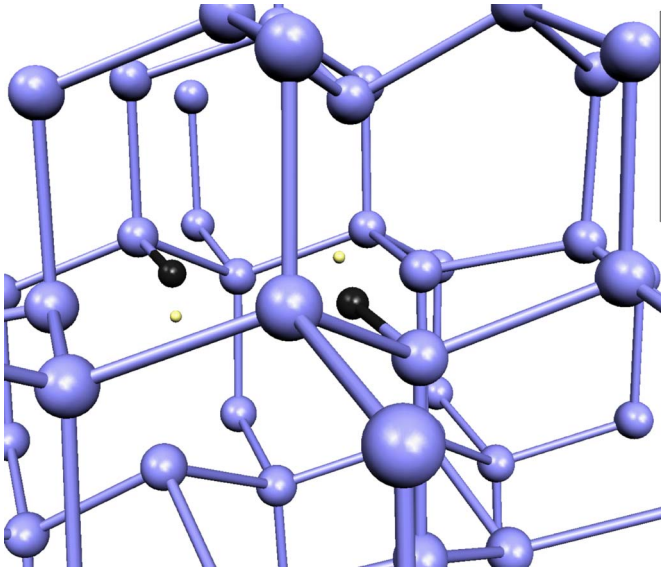

FIG. 10. (Color online) Structure of the H$V\cdot V$H complex. The hydrogen atoms are in black, the Si are the large gray (light blue) circles, and the two vacancy sites ares the small gray circles (light yellow).

Because both H atoms have plenty of free space to vibrate, their vibrational lifetimes are believed[9] to be similar to those of Si-H surface defects.

Figure 11 shows the localization plots of H$V\cdot V$H, D$V\cdot V$H, and D$V\cdot V$D. The calculated LVMs of H$V\cdot V$H consist of a doublet of stretch modes at 2092 cm^{-1} (measured:[9] 2072 cm^{-1}) and two doublets of wag modes at 594 cm^{-1} (infrared active) and 602 cm^{-1} (infrared inactive).

In the case of D$V\cdot V$H, the two stretch modes and the Si-H wag modes are LVMs, but the Si-D wag modes occur near a peak of the bulk Si phonon density of states and are therefore quite delocalized. As for D$V\cdot V$D, only the stretch modes are localized. Since the defects reconstruct very efficiently, there are no pLVMs associated with the Si neighbors.

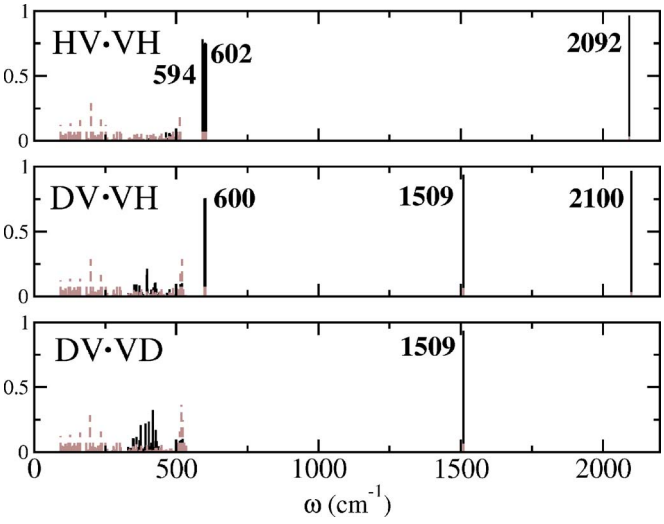

FIG. 11. (Color online) Localization plots of H$V\cdot V$H (top), D$V\cdot V$H (middle), and D$V\cdot V$D (bottom).

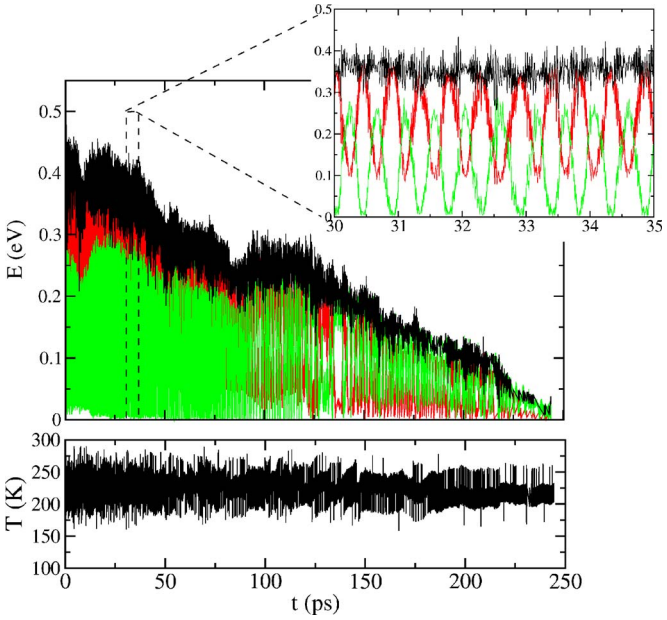

FIG. 12. (Color online) Decay of the stretch mode of H$V\cdot V$H for almost 850 000 time steps. The black curve is the sum of the energies of the two degenerate stretch modes in green and red (light and dark gray). The inset is a blowup of a 5 ps region. The black curve below the decay shows the instantaneous temperature of the supercell during the simulation.

Because of the very long lifetime of the Si-H stretch mode, the divacancy-dihydrogen complex is a computationally challenging problem. The low-temperature vibrational lifetime of the stretch mode has been observed[1] to be nearly 300 ps. With a 0.3 fs time step, this requires of the order of 1×10^6 MD time steps. Only one run was performed for each isotope. Since slow decays are independent of the initial conditions, we expect this to be sufficient.

Since the excited mode is degenerate, energy readily exchanges between the two stretch modes at 2092 cm^{-1}. This exchange occurs on a time scale much shorter than the decay process. Figure 12 shows the decay of H$V\cdot V$H at 200 K. This MD run involved almost 850 000 time steps. An exponential fit to this curve yields a lifetime of 187 ps, close to the 210 ps measured value at this temperature.[1] The black curve below the figure shows the actual temperature of the supercell as a function of time. As discussed in Sec. II, our cited temperature (T=200 K) does not include the increase of temperature $\Delta T\sim25$ K caused by the $3\hbar\omega/2$ excitation of the LVM.

An analysis of the energy of all the vibrational modes in the supercell does not suggest that a unique channel or even a few specific modes are involved. The decay is so slow that the other modes of the system remain in quasiequilibrium throughout the entire process. In particular, the wag modes at 594 and 602 cm^{-1} are not the primary receiving channels.

We also calculated the lifetimes of the high-frequency stretch modes of D$V\cdot V$H (2100 cm^{-1}) and D$V\cdot V$D (1509 cm^{-1}) at T=200 K. They are 117 and 106 ps, respectively. While no experimental data exists for D$V\cdot V$H, a 93 ps lifetime for D$V\cdot V$D was estimated[9] from the linewidth.

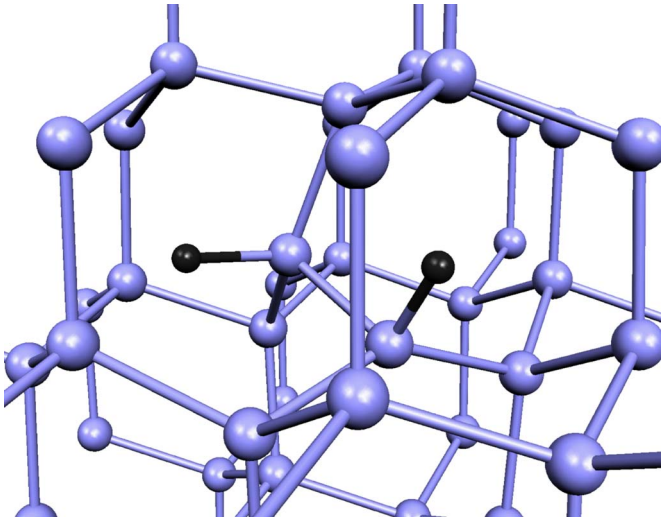

FIG. 13. (Color online) The IH_2 defect consists of a split Si self-interstitial (blue or light gray) and two H (or D) atoms (black).

4. IH_2 and ID_2

We investigated the IH_2 and ID_2 complexes because the experimental evidence suggests a strange isotope effect: the low temperature lifetimes of the high frequency stretch of IH_2 (1990 cm^{-1}) and ID_2 (1449 cm^{-1}) have been estimated from the linewidth[9] to be 11 and 18 ps, respectively. Upon deuteration, the frequency drops by nearly 600 cm^{-1} and therefore comes closer to the frequencies of the phonon bath. However, the vibrational lifetime nearly doubles, suggesting a reverse frequency-gap law. The structure of this defect is shown in Fig. 13. It consists of a Si self-interstitial and two H (or two D) atoms.

The localization plots of the defects are shown in Fig. 14. In IH_2, the Si-H stretch modes are at 2065 cm^{-1} (measured:[9] 1990 cm^{-1}) and the wag modes are calculated to be at 736 and 702 cm^{-1}. In ID_2, the stretch modes drop to 1481 cm^{-1} (measured:[9] 1449 cm^{-1}) and the wag modes shift below the Γ phonon. They show little local character at all. Both defects exhibit an almost identical resonant mode (perturbed Si-Si stretch mode) slightly above the Γ phonon.

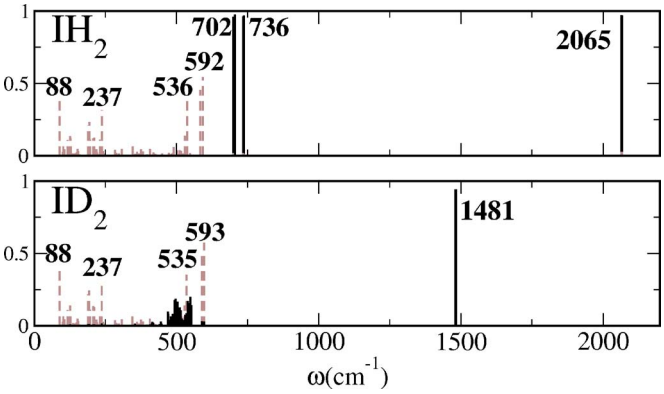

FIG. 14. (Color online) Localization plot of IH_2 (top) and ID_2 (bottom). The H- or D-related modes are shown with a solid (black) line, and the modes related to the Si neighbors are the dashed brown (gray) lines.

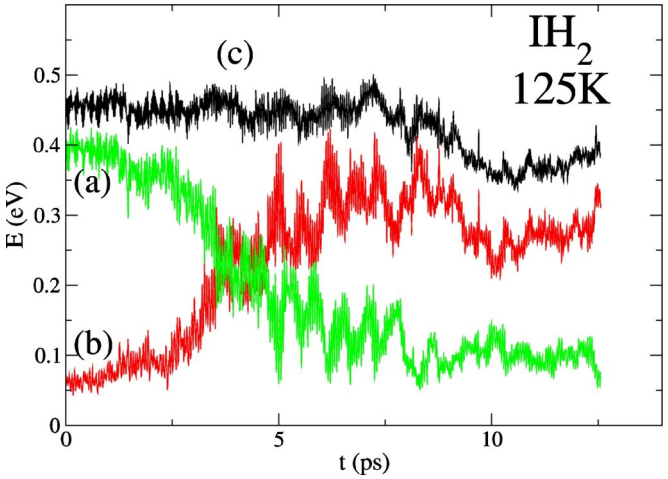

FIG. 15. (Color online) Curve (a) is the energy of the high frequency stretch of IH_2. Curve (b) is the sum of the energies of the 736, 702, and 592 cm^{-1} accepting modes. Curve (c) is the sum of (a) and (b).

The lifetime of the highest-frequency stretch mode of IH_2 and ID_2 were calculated at $T=125$ K, yielding lifetimes of 9.2 and 29 ps, respectively. The former lifetime is very close to the measured one while the latter is somewhat longer, but the increase in lifetime with H to D substitution is consistent with observations.

As shown in Fig. 15, the decay of the high-frequency stretch mode of IH_2 involves exclusively the localized modes at 736, 702, and 592 cm^{-1}. These are all doublets, and the two modes in each pair couple to each other. Thus, the decay of the stretch mode of IH_2 involves three localized phonons, with $2065 \rightarrow 736+702+592 cm^{-1}$.

On the other hand, the stretch mode of ID_2 has a much longer lifetime, as its wag modes drop below the Γ phonon and are much more delocalized. The only localized mode involved is the Si-S*i* resonant mode at 593 cm^{-1}. The remaining energy is dissipated into bulk (delocalized) phonons. As noted above, excited LVMs couple much stronger to other localized modes (LVMs, pLVMs, or resonant modes) than to bulk phonons.

B. The bizarre case of O_i

Interstitial oxygen is stable at a slightly puckered BC site, a structure known since 1950s.[35] Its asymmetric stretch at 1136 cm^{-1} is one of the best known lines in infrared spectroscopy. The calculated lowest-energy structure has a Si-O-Si angle of about 174°. On the average, it has D_{3d} symmetry[36] because O either rotates around the trigonal axis or tunnels through the BC site. The low-temperature lifetimes of a number of isotope combinations involving O_i have recently been measured by transient bleaching spectroscopy.[19] The experiments have focused on the large variations of the lifetime with the isotope substitutions involving O or its Si NNs.

The observed lifetimes are given in column 6 of Table III. Even though the structure of the defect is always the same,

TABLE III. The first column specifies the isotope composition. For example, "28-17-28" stands for ^{28}Si-^{17}O-^{28}Si. ω_1 and ω_3 are the symmetric stretch of the two Si NNs to O_i and the asymmetric stretch of O_i, respectively. The third and fourth columns are the measured and calculated frequencies. In the fifth column, $\Delta\omega=\omega_3-\omega_1$ is the frequency of the missing phonon needed to achieve the decay. The last two columns give the measured and calculated lifetimes T_1 of ω_3. (see Ref. 19 and references therein).

		ω (cm^{-1})			T_1 (ps)	
Isotopes	Mode	Expt.	Theor.	$\Delta\omega$ Expt.	Expt.	Theor.
28-17-28	ω_1	613	641			
	ω_3	1109	1158	496	4	7
28-16-28	ω_1	613	641			
	ω_3	1136	1187	523	11	10
29-16-28	ω_1	608	635			
	ω_3	1134	1185	526	19	15
30-16-28	ω_1	609	630			
	ω_3	1133	1183	530	28	22
30-16-30	ω_1	594	586			
	ω_3	1129	1146	535	28	

isotope substitutions that change the frequency by as little as 0.3% can change the lifetime by more than 100%. Furthermore, the asymmetric stretch of O_i has a longer lifetime in ^{30}Si-^{16}O-^{28}Si than ^{29}Si-^{16}O-^{28}Si which in turn is longer than in ^{28}Si-^{16}O-^{28}Si, an apparent violation of the frequency-gap law.

We calculated the lifetimes of the asymmetric stretch ω_3 at 200 K using the same approach as that for the H-related defects. We performed five MD runs for the shorter-lived LVMs (^{28}Si-^{17}O-^{28}Si and ^{28}Si-^{16}O-^{28}Si) and three for the longer-lived ones (^{29}Si-^{16}O-^{28}Si and ^{30}Si-^{16}O-^{28}Si). The measured and the calculated lifetimes are given in Table III.

The insight behind the strange isotope effects begins with an analysis of the accepting modes. Figure 2 in Ref. 19 shows a decay of the ω_3 mode of ^{28}Si-^{16}O-^{28}Si. The energy dissipated as ω_3 decays is absorbed by ω_1 (Si-Si symmetric stretch of the two Si NNs to O_i) and an optic mode at 524 cm^{-1}.

In all our simulations, and for all the isotope combinations, we find ω_1 to be a receiving mode. The key to understanding the isotope effects lies in the frequency of the missing phonon(s) $\Delta\omega=\omega_3-\omega_1$.

Figure 16 shows the calculated ω_3, ω_1, and the difference $\Delta\omega=\omega_3-\omega_1$ for the various isotopes combinations. In the case of ^{28}Si–^{16}O–^{28}Si, $\Delta\omega$ is at the peak of the phonon density of states, where many vibrational modes with the desired frequency are available. Hence, it has the shortest lifetime. $\Delta\omega$ shifts toward higher frequencies for ^{29}Si-^{16}O-^{28}Si and ^{30}Si-^{16}O-^{28}Si because ω_1 shifts toward lower frequencies while ω_3 remains essentially unchanged. The dramatic falloff in the phonon density of states implies that there are either very few modes available with the frequency $\Delta\omega$ or that two phonons are required. This causes the rapid increase in the vibrational lifetime of ω_3. The decay is a two-phonon process for ^{28}Si-^{16}O-^{28}Si but a three phonon process for ^{30}Si-^{16}O-^{28}Si.

IV. SUMMARY AND DISCUSSION

A first-principles approach to the calculation of vibrational lifetimes has been developed and applied to a range of LVMs in Si. The approach makes extensive use of the eigenvectors of the dynamical matrix. These vectors allow us to (a) identify all the localized modes in the system (LVMs, pLVMs, and resonant modes) and quantify their localization, (b) prepare the supercell in thermal equilibrium at the temperature T without requiring thermalization runs, (c) provide the excitation of the LVM under study, and (d) transform the Cartesian coordinates at every MD time step into normal-mode coordinates, thus allowing us to monitor the energy of every vibrational modes in system as a function of time at

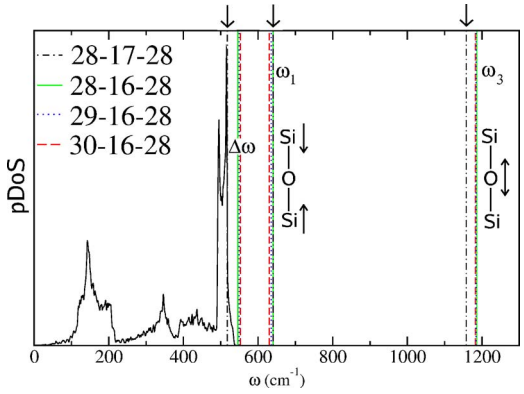

FIG. 16. (Color online) Calculated frequencies of ω_3 (asymmetric stretch of O_i), ω_1 (symmetric stretch of its two Si NNs), and the difference of these two frequencies $\Delta\omega$ for the various isotope combinations listed in the figure. Since some of the lines are too close to each other to be distinguishable, the reader is referred to Table III where the frequencies are listed. The arrow points to the lines corresponding to the 28-17-28 isotope combination, which has the shortest lifetime.

the desired temperature. This approach makes it possible to perform constant-energy MD runs with minimal temperature fluctuations without using a thermostat. The stability of the temperature of the supercell under these conditions is illustrated by the ~850 000 time steps MD run performed at $T=200$ K in the case of $HV\cdot VH$.

The vibrational lifetimes of highest-frequency LVM of H_{BC}^{+}, D_2^*, HD^*, DH^*, H_{BC}^{+}, D_{BC}^{+}, $HV\cdot VH$, $DV\cdot VH$, $DV\cdot VD$, IH_2, ID_2, and various O and Si isotopic combinations of O_i have been calculated and the decay channels analyzed. The theoretical predictions are always close to the values measured by transient bleaching spectroscopy at various temperatures: H_2^*, H_{BC}^{+}, $HV\cdot VH$, and all the O_i isotope combinations. The calculated lifetimes tend to be longer than those estimated from measurements of the linewidth: D_2^*, D_{BC}^{+}, $DV\cdot VD$, IH_2, and ID_2. Note that the lifetime of H_2^* measured by transient bleaching spectroscopy[1] (4.2 ps) is also longer than the lifetime estimated from the linewidth[9] (1.9 ps).

The temperature dependences of the calculated lifetimes match the measured ones above $T\sim 75$ K but fail to reproduce the plateau observed experimentally below that value (Fig. 4 in Ref. 18). This plateau is a zero-point motion effect. Indeed, the anharmonic couplings no longer change when all the receiving modes reach their zero-point oscillation amplitudes. In classical MD, the amplitudes continue to decrease, the oscillations become harmonic, the modes no longer couple to each other, and all the lifetimes become very long.

Since our calculations allow us to identify all the localized modes in the system (LVMs, pLVMs, and resonant modes) as well as monitor the amplitudes and energies of all the normal modes of the cell, we have gained insight into the decay mechanisms.

A study[13] of the lifetimes of H-related wag modes has established that the vibrational lifetimes increase exponentially with the decay order (frequency-gap law), and the decay order increases with the separation between these LVMs and the bulk phonon bands.

The frequency-gap law works well for these wag modes as there are few or no localized modes into which they can decay, but it is only an upper bound for the lifetimes of high-frequency LVMs, which sometimes decay much faster than the law predicts. Our results show that LVMs couple much stronger to *localized* lower-frequency modes than to delocalized bulk modes. These localized modes can be other LVMs, resonant modes, or pLVMs. Further, the existence of LVMs can also lower the decay order.

Examples include the 2062 cm^{-1} mode of H_2^*, which decays into a LVM and a pLVM, while the longer-lived (but lower-frequency) mode of D_2^* involves only one LVM (and bulk phonons). As shown in Fig. 9, the 1998 cm^{-1} mode of H_{BC}^{+} cannot decay into fewer than four phonons. However, its lifetime is very short as it decays into pLVMs and resonant modes. Note that H_{BC}^{+} is the only charged defect considered here, and this may have an impact on the coupling strength as well. Finally, the lifetime of the high-frequency LVM of IH_2 is about one-third that of ID_2. The former couples exclusively to localized modes, while the latter couples to one LVM and delocalized phonons.

On the other hand, the high-frequency mode of $HV\cdot VH$ could also decay into four phonons, but none of those are localized resulting in a much longer lifetime. Thus, it is impossible to estimate the vibrational lifetime of a high-frequency LVM without prior knowledge of the entire vibrational spectrum of the defect. This can only be obtained from first-principles theory, because the spectrum involves vibrational modes that cannot be observed experimentally.

The larger coupling strength to localized vs bulk modes may be the reason why the fits[1,6] of the measured temperature dependence of the lifetimes to the formula proposed by Nitzan *et al.*[11] and Egorov and Skinner[12] predict strange decay orders, such as a six phonon process for an 8 ps lifetime and a five phonon process for a 295 ps one. The application of the formula of Nitzan *et al.* in Refs. 1–6 ignored the existence of other localized modes. A complication arises from the fact that some of the modes localized on the defect couple strongly to the excited LVM (such as the symmetric stretch of the Si NNs to O_i), while others couple very weakly at best (such as the Si-H wag modes in $HV\cdot VH$). Our calculations also suggest that more than one decay channel is at play in the case of the very long lifetime of $HV\cdot VH$, and therefore that the single-channel fit is not sufficient.

We also note that estimating the vibrational lifetimes of high-frequency LVMs from the linewidth only gives a lower limit to the actual lifetime. This is established experimentally in the case of H_2^*, and all our calculations predict longer lifetimes than the ones obtained from linewidth measurements.

Finally, it is quite remarkable that classical MD simulations are capable of predicting vibrational lifetimes even at relatively low temperatures. The quantized nature of phonons affects the classical predictions only when the zero-point energies dominate the interactions.

ACKNOWLEDGMENTS

The work of S.K.E. is supported in part by a grant from the R.A. Welch Foundation and a contract from the National Renewable Energy Laboratory. Many thanks to Texas Tech's High Performance Computer Center for generous amounts of CPU time.

*Electronic address: stefan.estreicher@ttu.edu

[1] G. Lüpke, X. Zhang, B. Sun, A. Fraser, N. H. Tolk, and L. C. Feldman, Phys. Rev. Lett. **88**, 135501 (2002).

[2] T.-C. Shen, C. Wang, G. C. Abeln, J. R. Tucker, J. W. Lyding, Ph. Avouris, and R. E. Walkup, Science **268**, 1590 (1995).

[3] A. Stesmans, Phys. Rev. B **61**, 8393 (2000); J. Appl. Phys. **88**, 489 (2000).

[4] J. W. Lyding, K. Hess, and I. C. Kizilyalli, Appl. Phys. Lett. **68**, 2526 (1996).

[5] L. C. Feldman, G. Lüpke, and N. H. Tolk, Solid State Phenom.

95–96, 123 (2004).
[6] M. Budde, G. Lüpke, C. P. Cheney, N. H. Tolk, and L. C. Feldman, Phys. Rev. Lett. **85**, 1452 (2000).
[7] G. Lüpke, N. H. Tolk, and L. C. Feldman, J. Appl. Phys. **93**, 1 (2003).
[8] M. Budde, C. P. Cheney, G. Lüpke, N. H. Tolk, and L. C. Feldman, Phys. Rev. B **63**, 195203 (2001).
[9] M. Budde, G. Lüpke, E Chen, X. Zhang, N. H. Tolk, L. C. Feldman, E. Tarhan, A. K. Ramdas, and M. Stavola, Phys. Rev. Lett. **87**, 145501 (2001).
[10] F. Widulle, T. Ruf, M. Konuma, I. Silier, W. Kriegseis, M. Cardona, and V. I. Ozhogin, Solid State Commun. **118**, 1 (2001).
[11] A. Nitzan and J. Jortner, Mol. Phys. **25**, 713 (1973); A. Nitzan, S. Mukamel, and J. Jortner, J. Chem. Phys. **60**, 3929 (1974).
[12] S. A. Egorov and J. L. Skinner, J. Chem. Phys. **103**, 1533 (1995).
[13] B. Sun, G. A. Shi, S. V. S. Nageswara Rao, M. Stavola, N. H. Tolk, S. K. Dixit, L. C. Feldman, and G. Lüpke, Phys. Rev. Lett. **96**, 035501 (2006).
[14] J. Fabian and P. B. Allen, Phys. Rev. Lett. **77**, 3839 (1996).
[15] S. R. Bickham and J. L. Feldman, Phys. Rev. B **57**, 12234 (1998).
[16] F. H. Stillinger and T. H. Weber, Phys. Rev. B **31**, 5262 (1985).
[17] R. Biswas, Y.-P. Li, and B. C. Pan, Appl. Phys. Lett. **72**, 3500 (1998).
[18] D. West and S. K. Estreicher, Phys. Rev. Lett. **96**, 115504 (2006).
[19] K. K. Kohli, G. Davies, N. Q. Vinh, D. West, S. K. Estreicher, T. Gregorkiewicz, I. Izeddin, and K. M. Itoh, Phys. Rev. Lett. **96**, 225503 (2006).
[20] D. Sánchez-Portal, P. Ordejón, E. Artacho, and J. M. Soler, Int. J. Quantum Chem. **65**, 453 (1997).
[21] E. Artacho, D. Sánchez-Portal, P. Ordejón, A. García, and J. M. Soler, Phys. Status Solidi B **215**, 809 (1999).
[22] L. Kleinman and D. M. Bylander, Phys. Rev. Lett. **48**, 1425 (1982).
[23] D. M. Ceperley and B. J. Alder, Phys. Rev. Lett. **45**, 566 (1980).
[24] S. Perdew and A. Zunger, Phys. Rev. B **23**, 5048 (1981).
[25] O. F. Sankey and D. J. Niklewski, Phys. Rev. B **40**, 3979 (1989); O. F. Sankey, D. J. Niklewski, D. A. Drabold, and J. D. Dow, *ibid.* **41**, 12750 (1990).
[26] S. Baroni, P. Giannozzi, and A. Testa, Phys. Rev. Lett. **58**, 1861 (1987).
[27] X. Gonze, Phys. Rev. A **52**, 1096 (1995); X. Gonze and C. Lee, Phys. Rev. B **55**, 10355 (1997).
[28] J. M. Pruneda, S. K. Estreicher, J. Junquera, J. Ferrer, and P. Ordejón, Phys. Rev. B **65**, 075210 (2002).
[29] S. Nose, Mol. Phys. **52**, 255 (1984).
[30] S. Nose, J. Chem. Phys. **82**, 511 (1984).
[31] J. D. Holbech, B. Bech Nielsen, R. Jones, P. Sitch, and S. Öberg, Phys. Rev. Lett. **71**, 875 (1993).
[32] A. S. Barker, Jr., and A. J. Sievers, Rev. Mod. Phys. **47**, S1 (1975).
[33] S. K. Estreicher, D. West, J. Goss, S. Knack, and J. Weber, Phys. Rev. Lett. **90**, 035504 (2003); S. K. Estreicher, D. West, and M. Sanati, Phys. Rev. B **72**, 121201(R) (2005).
[34] M. Budde, Ph.D. thesis, University of Aarhus, 1998.
[35] W. Kaiser, W. P. H. Keck, and C. F. Lange, Phys. Rev. **101**, 1264 (1956).
[36] See *Oxygen in Silicon*, edited by F. Shimura (Academic, Boston, 1994); *Early Stages of Oxygen Precipitation in Silicon*, edited by R. Jones (Kluwer, Dordrecht, 1996).